Journal of the Mechanical Behavior of Biomedical Materials 76 (2017) 30–37

Contents lists available at ScienceDirect

Journal of the Mechanical Behavior of Biomedical Materials

journal homepage: www.elsevier.com/locate/jmbbm

Lamellae spatial distribution modulates fracture behavior and toughness of african pangolin scales

Michael J. Chon[a], Matthew Daly[a], Bin Wang[b,c], Xianghui Xiao[d], Alireza Zaheri[e], Marc A. Meyers[b], Horacio D. Espinosa[a,e,*]

[a] Department of Mechanical Engineering, Northwestern University, Evanston, IL 60062, USA
[b] Department of Mechanical and Aerospace Engineering, University of California, San Diego, CA 92093, USA
[c] Shenzhen Institute of Advanced Technology, Chinese Academy of Sciences, Shenzhen, People's Republic of China
[d] Advanced Photon Source, Argonne National Laboratory, Lemont, IL 60439, USA
[e] Theoretical and Applied Mechanics Program, Northwestern University, Evanston, IL 60062, USA

ARTICLE INFO

Keywords:
Pangolin scale
Fracture toughness
Hierarchical structure
Bio-inspired design principles
Biomaterials

ABSTRACT

Pangolin scales form a durable armor whose hierarchical structure offers an avenue towards high performance bio-inspired materials design. In this study, the fracture resistance of African pangolin scales is examined using single edge crack three-point bend fracture testing in order to understand toughening mechanisms arising from the structures of natural mammalian armors. In these mechanical tests, the influence of material orientation and hydration level are examined. The fracture experiments reveal an exceptional fracture resistance due to crack deflection induced by the internal spatial orientation of lamellae. An order of magnitude increase in the measured fracture resistance due to scale hydration, reaching up to ~ 25 kJ/m^2 was measured. Post-mortem analysis of the fracture samples was performed using a combination of optical and electron microscopy, and X-ray computerized tomography. Interestingly, the crack profile morphologies are observed to follow paths outlined by the keratinous lamellae structure of the pangolin scale. Most notably, the inherent structure of pangolin scales offers a pathway for crack deflection and fracture toughening. The results of this study are expected to be useful as design principles for high performance biomimetic applications.

1. Introduction

Through millions of years of evolution, biological organisms have developed a variety of strategies for their protective systems in order to increase their survivability in response to environmental constraints. In this regard, natural dermal armors have been one of the most diverse protection systems employed by species against their predators (Yang et al., 2013b). These armors, which are commonly protecting the softer body organs, can be found as rigid shell materials such as nacre (Mayer, 2005) in mollusks or segmented flexible armors atop the skin, as in fish (Zhu et al., 2012). The latter armors, which commonly present in the form of scales, are found in a wide range of animals such as reptiles (Abdel-Aal and El Mansori, 2011), mammals (Chen et al., 2011) and most fish (Porter et al., 2016). The main differences in between these armors are rooted in their hierarchical structure and compositions, which make them differentiable from each other. For example, in the case of fish, collagen-based biopolymer fibers (Dastjerdi and Barthelat, 2015) play a key role in providing flexibility, whereas nacre is comprised primarily of mineral tablets (Espinosa et al., 2009) which provides significant rigidity and excellent crack-arresting properties (Barthelat et al., 2007).

Historically, natural armors have served as a source of design inspiration for human protective systems. For example, several warrior armor concepts are constructed from overlapping metal plates, which are sewn into thick fabrics (Arciszewski and Cornell, 2006), in a manner analogous to scaled armors. Conceptual inspirations from natural armors require a systematic categorization to contextualize the performance space of these systems, and to connect structure-property relationships. To this end, armors are classified based on their microstructural designs principles as multilayered structures with inner soft layers as in fish (Dastjerdi and Barthelat, 2015), hard mineralized tiles connected with organic fibrils as in armadillos (Chen et al., 2011), and complex arrangements of sutures between hard plates as in turtle shells (Krauss et al., 2009). In all designs, the soft layers as well as joints are made of collagen biopolymers. Collagen is made of polypeptide chains and is a very common building protein blocks in many tissue systems. Besides collagen, keratin is another structural protein, which is found mostly in vertebrate animals (Meyers et al., 2008; Wang et al.,

* Corresponding author at: Department of Mechanical Engineering, Northwestern University, Evanston, IL 60062, USA.
E-mail address: espinosa@northwestern.edu (H.D. Espinosa).

http://dx.doi.org/10.1016/j.jmbbm.2017.06.009
Received 15 April 2017; Received in revised form 5 June 2017; Accepted 7 June 2017
Available online 10 June 2017
1751-6161/

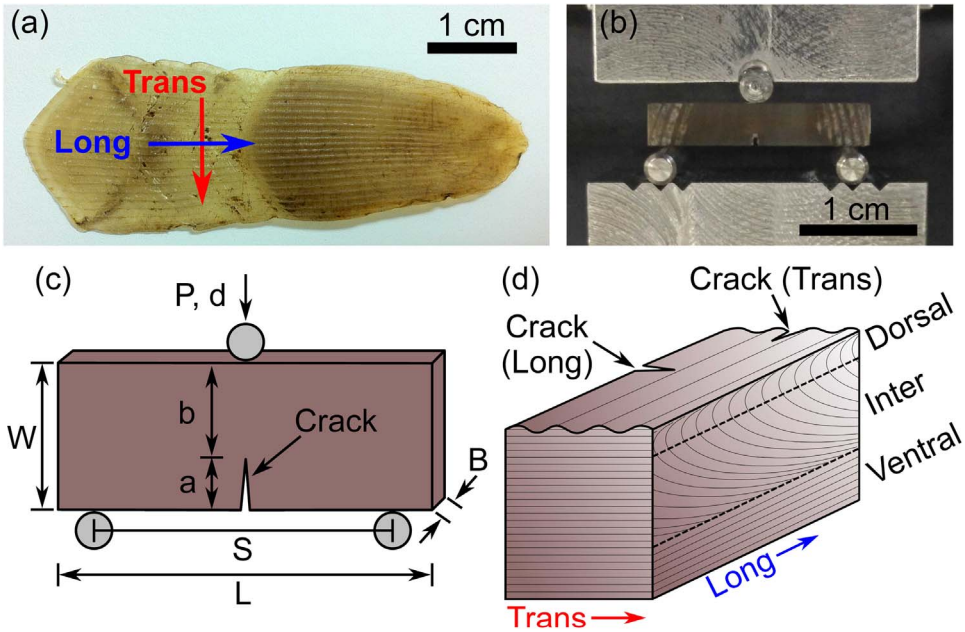

Fig. 1. (a) A photograph of a typical scale of the African tree pangolin. The transverse (Trans) and longitudinal (Long) material directions are indicated. (b) A typical single edge cracked TPB specimen positioned within the loading frame. (c) The geometric parameters used in fracture resistance analysis. (d) A perspective cross-section schematic of the pangolin scale revealing the layering patterns of keratinous lamellae which form the dorsal, intermediate (inter) and ventral regimes. This schematic has been adapted from Liu et al. (2016a), with permission. The orientation of the edge crack relative to the material directions is indicated. (For interpretation of the colors used in these schematics, the reader is referred to the web version of this article).

2016a). Several keratin-based scale type materials at the micrometer level were identified in biological organs such as bird beaks (Seki et al., 2006) and on the cortex surface of quill tips (Yang et al., 2013a). Within the realm of mammalian creatures, the pangolin represents a unique animal whose dorsal surface is fully covered with large, overlapping keratinous scales (Spearman, 1967). However, in contrast to fish, the scales are individually connected to the skin, which improves general mobility.

Pangolins are one of few mammalian species with protective armor and, the only known mammal with overlapping scales (Wang et al., 2016a). These species, which are found in tropical climates, can be divided into two main families (Wang et al., 2016b). The first group inhabits underground burrows and one representative species is the Chinese pangolin (*Manis pentadactyla*). The second group, known as the arboreal type, is comprised of species such as the African tree pangolin (*Manis tricuspis)*, which possesses comparatively larger scales, and the ability to flex their bodies to climb trees. Recently, an extensive body of research was published on characterizing the material properties of scales from these two families of pangolin (Liu et al., 2016a, 2016b; Wang et al., 2016b). Both types of pangolin scales showed similar microstructural design with three distinct regions of lamellae arrangement throughout the thickness. The top and bottom regions, which are called dorsal and ventral, respectively, are composed of a crossed lamellar arrangement of flattened keratinous cells with an interlocking nanosuture structure at the interfaces of lamellae. However, keratin cells are less flat in the intermediate (inter) region and are continuously tilted towards the outer scale surface. This kind of tilt alignment of laminates are also reported in other tissue level materials such as crayfish mandibles (Bentov et al., 2012) and tooth enamel (Boyde, 1964). These pangolin scales are reported to exhibit transverse isotropy in the plane of the scale surface at an ambient humidity (Wang et al., 2016b). These scales also exhibit significant viscoelasticity, which reveals a strain rate dependency characteristic. Under hydrated conditions, mechanical tests have reported less rate dependency and a higher anisotropy (Liu et al., 2016a).

One of the most important functions underpinning the biological role of all natural armors is to provide resistance for contact deformation and damage. However, armor systems show a trade-off between protection and mobility for longer endurability (Arciszewski and Cornell, 2006). This varies in accordance to species habitat and behavior. In most of the natural armors like fish scale, the outer layer is highly mineralized to resist penetration, and inner layers are softer and tougher. This compositional variation manifests as a gradient in modulus and hardness, which has been shown to provide an efficient biological design for crack arresting and high energy dissipation (Meyers et al., 2012; Sherman et al., 2016). In contrast, pangolin scales possess a homogenous composition with no mineral content (Spearman, 1967). Moreover, the stiffness and hardness properties are uniform without any gradient throughout the thickness of the scales, despite the underlying heterogeneity of the keratinous lamellae structure. Within the context of armor performance, this apparent disconnect between mechanical properties and structure motivates an investigation of crack propagation and the toughening mechanisms in pangolin scales. In this study, we present an investigation of the fracture behavior of African pangolin scales using single edge crack three-point bend (TPB) tests, which are implemented to assess the crack resistance curves of the scales. The effects of hydration and lamellae orientation are examined and post-mortem analysis of the pangolin scales is conducted to ascertain the structure-property relationships of the fracture behavior.

Within the larger context of armor design, the aforementioned spatial gradient in the structural design and mechanical properties of natural armors can lead to better load transfer and efficient stress-field redistribution, resulting in significant protection enhancement (Bruet et al., 2008; Liu et al., 2016c). This concept has been previously leveraged in many synthetic functionally graded material systems developed for wear and penetration resistant surfaces (Chintapalli et al., 2014) in applications such as: flexible electronics (Suresh, 2001), personal armors (Huang et al., 2011), thermal barrier coatings (Koizumi and Niino, 1995), and other commercial products (Wang et al., 2016a). In this regard, a detailed investigation of the fracture toughness of pangolin scales can be a source of inspiration for manufacturing new classes of lightweight armors.

2. Materials and methods

2.1. Sample preparation

Samples for fracture resistance measurements were laser cut from dry African pangolin scales. The scales were extracted from the host animal, which had died from natural causes and its pelt was treated with salt before storage. A photograph of a typical pangolin scale along with the relevant material directions is presented in Fig. 1a. Prior to mechanical testing, each sample was ground to nominal dimensions of 3.5 × 1 × 20 mm (W × B × L). During this process, any regions of the

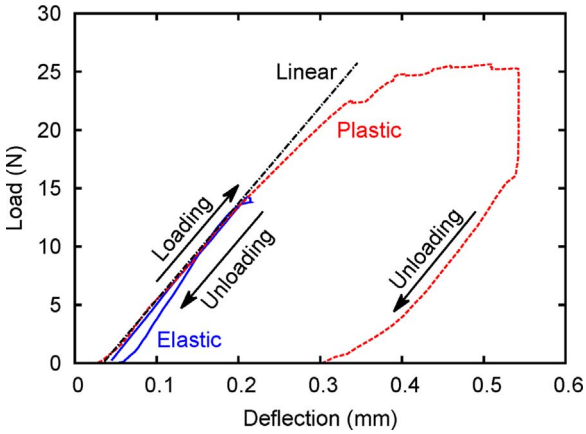

Fig. 2. A typical load-deflection curve which is acquired during TPB fracture tests of the pangolin scales. Elastic and plastic load-unload cycles are indicated. (For interpretation of the references to color in this figure, the reader is referred to the web version of this article).

sample that were singed due to laser cutting were removed. A thin diamond-tipped saw was used to introduce a single edge notch (~ 1 mm) perpendicular to the edge of the sample. After notching, the surface was further polished using a 0.3 μm Al_2O_3 slurry and immediately prior to testing, the notch was sharpened with a fresh razor blade to define a crack. Fig. 1b provides an image of a pangolin scale, which has been prepared for TPB testing. A schematic of the relevant geometric parameters with respect to the cracked pangolin scale samples is provided in Fig. 1c. Pangolin scales are known to be comprised of a heterogeneous layering of keratinous lamellae (Liu et al., 2016a; Wang et al., 2016b), which are readily visible in longitudinal cross-sections. Liu et al. (2016a) report three distinct regimes of lamellae stacking: dorsal, intermediate (inter), and ventral. In the dorsal region, lamellae are stacked with a tight curvature. The radius of curvature of the lamellae gradually increases through the intermediate region, approaching a flat stacking profile in the ventral regime. A perspective cross-section of these lamellae structures is provided in Fig. 1d. In order to understand the effects of lamellae organization on fracture behavior, samples were prepared to measure the fracture resistance of pangolin scales in the longitudinal and transverse orientations. The orientation of the single edge cracks relative to the transverse and longitudinal directions is indicated in the figure. A naming convention was established to differentiate between cracked sample orientations. Trans and Long refer to cracked samples whose TPB-induced tensile stress-fields are aligned to the transverse and longitudinal orientations, respectively (Fig. 1d). In this manner, the nomenclature of the induced stress-field is consistent with uniaxial testing measurements previously reported (Liu et al., 2016a; Wang et al., 2016b), permitting a direct comparison of results.

In addition to consideration of orientation effects, the degree of hydration is reported to cause significant changes in the mechanical properties of pangolin scales (Liu et al., 2016a; Wang et al., 2016b). Consequently, fracture resistance measurements of the pangolin scale samples were collected under both ambient and fully hydrated conditions. The relative humidity was measured using a resistance-type sensor to range between ~ 20–30% in the laboratory for all ambient tests. Hydrated samples were kept in deionized (DI) water for 100 h prior to testing. It was observed that these samples became fully saturated such that no additional mass change was measured after 72 h in DI water. With respect to the sample naming convention, the ambient and hydrated samples are denoted by the subscripts "a" and "h". For example, the label Trans_a refers to a transversely loaded pangolin scale which has an ambient level of hydration.

2.2. Fracture resistance measurements

The fracture resistance of the pangolin scales was evaluated following the ASTM E1820 (ASTM(E1820-15a), 2015) standard which permits a direct assessment of the *J*-integral using TPB testing of single edge cracked specimens. The *J* parameter is relevant as it may be used to capture inelastic toughening at a crack-tip, which is known to play an important role in the fracture behavior of biomaterials. This approach has been used extensively to study fracture resistance in nacre (Barthelat and Espinosa, 2007) and other biological materials, including bass scales (Browning et al., 2013; Dastjerdi and Barthelat, 2015; Vernerey and Barthelat, 2014; Zhu et al., 2012; Zhu et al., 2013), alligator gar (Yang et al., 2013b, 2013c), the carapace of turtle shells (Achrai and Wagner, 2013; Balani et al., 2011; Damiens et al., 2012), and armadillos (Achrai and Wagner, 2013; Chen et al., 2011). The pre-notched samples were placed onto a miniature loading stage (Ernest F. Fullam, Inc., Latham, NY) to conduct displacement-controlled TPB tests. The applied load, *P*, was measured using an in-line 25 N load cell with a 1 mN resolution while the deflection, *d*, was measured by a linear variable differential transformer, possessing a resolution of 1 μm. The stage was placed under an optical microscope fitted with a CCD camera to acquire images of the crack extension during testing.

A typical load-displacement curve from a TPB test is shown in Fig. 2. When the material is loaded within the elastic regime (blue curve), the curve is linear and reversible upon unloading. There is no observable extension of the pre-crack or irreversible deformation of the material within this regime. When the material is loaded beyond the elastic regime (red curve), there is sufficient load on the material to induce plasticity – evidenced by a region of permanent deformation akin to a process zone around the crack-tip – and crack propagation. This process zone is visible in photographs as a region of localized flow which is likely facilitated by rearrangement of the internal lamellae in response to the tensile strain in front of the crack-tip (see Section 3.3). The onset of plasticity coincides with a deviation from linearity in the load-displacement curve and unloading of the sample results in a hysteresis, indicating energy dissipation. It should be noted that compliance in the stage and friction between moving parts contribute towards the hysteresis in the load-displacement curves, though the experimental errors introduced by these mechanisms are small compared to the energy dissipated by the material via plasticity and crack extension. Due to the high stiffness of the testing stage ($k = 2.5$ N/μm), and the relatively low loadings, deflection measurement errors due to machine compliance effects were assumed to be negligible.

J may be calculated at any point *i* along the load-displacement curve using the following formula:

$$J_{(i)} = J_{el(i)} + J_{pl(i)} \tag{1}$$

where J_{el} and J_{pl} are the elastic and plastic components of *J*, respectively (ASTM(E1820-15a), 2015). The elastic component, J_{el}, is a function of the stress intensity factor, K_i, and plane strain modulus, E', of the sample:

$$J_{el(i)} = K_{(i)}{}^2/E'; \quad E' = E/(1-\nu^2) \tag{2}$$

and

$$K_{(i)} = \left[P_i S/(BW^{\frac{3}{2}})\right] f(a_i/W), \tag{3a}$$

$$f(\bar{a}_i = a_i/W) = \frac{3\sqrt{\bar{a}_i}\,[1.99 - \bar{a}_i(1-\bar{a}_i)(2.15 - 3.93\bar{a}_i + 2.7\bar{a}_i{}^2)]}{2(1+2\bar{a}_i)(1-\bar{a}_i)^{3/2}}, \tag{3b}$$

where a_i is the crack length, and the remaining parameters are as defined in Fig. 1c. The dimensionless function $f(\bar{a}_i = a_i/W)$ is given by the above equation.

In an earlier study, the elastic moduli of African pangolin scales were measured in ambient humidity to be 1.2 and 1.0 GPa, in the

transverse and longitudinal orientation, respectively, and 315 MPa for both orientations in a hydrated state (Wang et al., 2016b). Under an isotropic assumption, the plane strain modulus of a material may be calculated using the Poisson's ratio, ν. Taking Eq. (2) and assuming a Poisson's ratio of 0.4, which is reported in other keratin-based biomaterials (Kasapi and Gosline, 1997), the plane strain moduli may be calculated as 1.4 ($Long_a$) and 1.2 GPa ($Trans_a$), and 375 MPa for both orientations in the hydrated condition.

The plastic component of the fracture resistance, J_{pl}, is a function of the area under the load-displacement curve, A_{pl}, and the ligament length, $b = W - a$, and is calculated as:

$$J_{pl(i)} = \left[J_{pl(i-1)} + \left(\frac{2}{b_{(i-1)}}\right)\left(\frac{A_{pl(i)} - A_{pl(i-1)}}{B}\right)\right]\left[1-\left(\frac{a_{(i)} - a_{(i-1)}}{b_{(i-1)}}\right)\right] \quad (4)$$

The unloading compliance of the pangolin scales, $C = \Delta d/\Delta P$ (i.e., the slope of the unload/reload curve), was observed to remain constant during TPB testing. Therefore, the incremental increase in plastic toughening can be estimated directly from the load-displacement curve, after correcting for elastic effects, using the following trapezoidal approximation:

$$\Delta A_{pl(i)} = A_{pl(i)} - A_{pl(i-1)} = \frac{(P_{(i)} + P_{(i-1)})(d_{(i)} - d_{(i-1)})}{2} \quad (5)$$

2.3. Monitoring of crack propagation

In order to calculate the fracture resistance of the pangolin scales, direct monitoring of the crack extension, Δa, during TPB tests is required. Digital image correlation was implemented to determine the position of the crack-tip, using a procedure reported in Barthelat and Espinosa (2007). In this technique, the vertical displacement fields around a crack-tip are used to estimate the shape of an advancing crack-tip. Fig. 3 illustrates this procedure in further detail. Vertical displacements are extracted from the isosurfaces of Fig. 3a along a path in the vicinity of the crack-tip (dashed-line). The extracted displacement profile is then fit to a parabolic function to determine the position of the crack-tip. Fig. 3b illustrates the propagation of the crack-tip at increasing loads during TPB tests. The calculated crack extensions are then used to determine the components of J, as outlined in the preceding subsection.

2.4. Post-mortem analysis

Optical images of the sample surface before and after testing were recorded to document the crack extension and surface morphology around the regions of interest. Images were stitched together using FIJI (Schindelin et al., 2012) to create a composite montage of the sample, from which key dimensions such as initial crack length, a_o, were ascertained. A white light interferometer (Zygo NewView 7000) was used to measure the topology change of the sample due to crack extension. Post-mortem electron imaging of the pangolin scales was performed using a scanning electron microscope (SEM) (FEI Nova 600). The TPB-loaded pangolin scales were manually broken after testing to reveal the cross-section fracture surface features. Prior to SEM imaging, a thin coating of osmium (~ 8 nm) was deposited onto the sample surface using an osmium plasma coater (OPC-60A, SPI Supplies) to reduce sample charging. For a select number of samples, high resolution X-ray computerized tomography (microCT) images were acquired at Argonne National Labs (Lemont, IL) to characterize the crack profile without introducing additional damage to the sample. Cross-sectional images were reconstructed from raw X-ray projections using TomoPy (Gursoy et al., 2014), which were then used to render 3D models of the crack profile using Amira software(FEI).

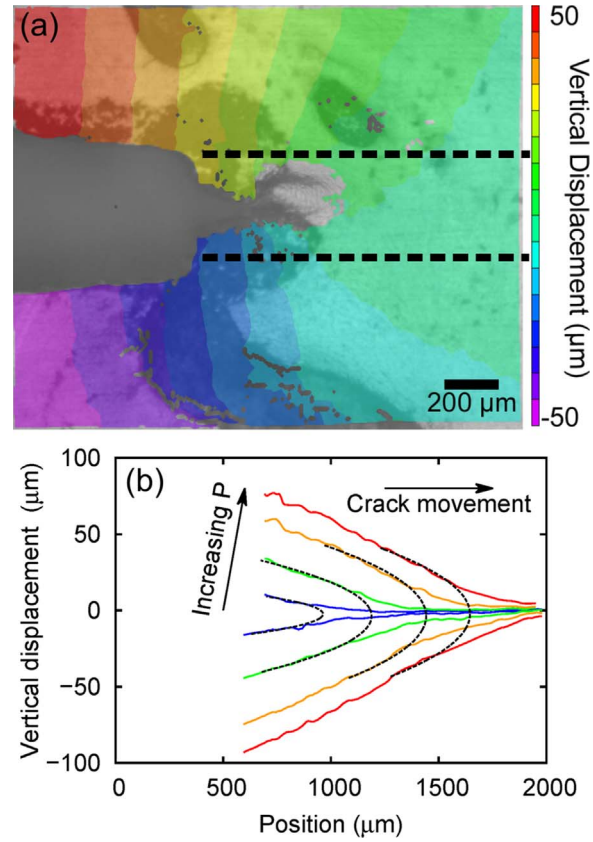

Fig. 3. (a) A digital image correlation map revealing isosurfaces of equivalent vertical displacement. These isosurfaces are used to generate a vertical displacement profile, which is collected along the dashed-line. The collected displacement profiles are fit to a parabolic function to track crack-tip propagation. (b) The crack-tip propagation at increasing loads. The parabolic fit is shown as the dashed-line. (For interpretation of the color scheme used in the plots of this figure, the reader is referred to the web version of this article).

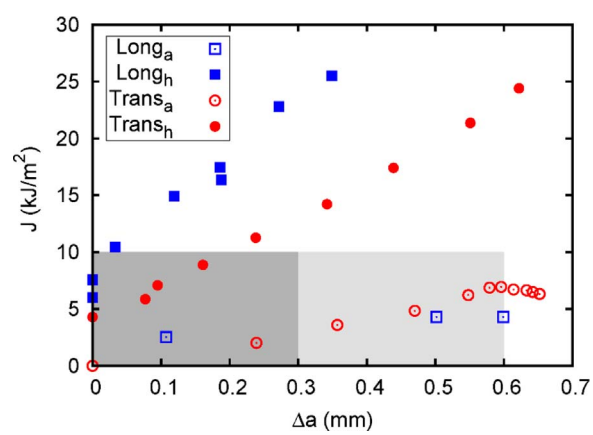

Fig. 4. The measured fracture resistance curves of the pangolin scales. J values are plotted for the transverse and longitudinal orientations for pangolin scales in an ambient and hydrated condition. The shaded areas indicate the regions where J measurements are considered to be geometry-independent. The darker region denotes the geometry-independent region for ambient samples and the lighter region for the hydrated scales. (For interpretation of the color scheme used in this plot, the reader is referred to the web version of this article).

3. Results and discussion

3.1. Fracture resistance curves

The measured fracture resistance (J-R) curves from TPB tests of the pangolin scales are reported in Fig. 4. The J values presented in this

figure represent the measurement window for each sample condition, which is limited by the initiation of unstable crack propagation in the pangolin scale. As shown in the figure, the J values for the scales tested at an ambient hydration level have peak toughness values of 4.3 and 6.3 kJ/m^2 for the longitudinal and transverse orientations, respectively. Significantly, in the hydrated condition, a large increase in the fracture resistance is measured with J reaching values as high ~ 25 kJ/m^2 in both material orientations, which represents an order of magnitude increase in material toughness. This trend is qualitatively consistent with toughness increases observed by Liu et al. (2016a) for uniaxial tensile studies of pangolin scales. The measurement is also consistent with generalized trends for the effects of hydration on toughness in biomaterials (Meyers and Chen, 2014). Additionally, there appears to be a more pronounced anisotropy in the hydrated pangolin scales, which is supported by similar observations in mechanical studies performed by Liu et al. (2016a). It should be noted that in the hydrated case, the high J values exceeded the limits defined by the ASTM standard (ASTM(E1820-15a), 2015) for geometry-independent measurements. As defined by the standard, the limits on J-controlled crack growth may be described by the following criteria:

$$J_{max} = min(b_o\sigma_Y/10 \;\; or \;\; B\sigma_Y/10) \tag{6}$$

$$\Delta a_{max} = 0.\,25b_o, \tag{7}$$

where σ_Y is the material yield stress, and b_o = W-a_o. Taking σ_Y as 80 and 40 MPa (Liu et al., 2016a) for the ambient and hydrated conditions, respectively, a conservative estimate of $J_{max} \approx 10$ kJ/m^2 may be calculated for both orientations. Similarly, Δa_{max} is determined to be ~ 0.3 and 0.6 mm for the ambient and hydrated conditions, respectively. The limiting boundaries of J-controlled crack growth are indicated in the figure. It is worth mentioning that the validity of Eqs. (6) and (7) to various biomaterials needs to be ascertained. Furthermore, while the usage of larger samples could extend the aforementioned limits, the thickness of the pangolin scale limits the geometry-independent window of J measurement, which is an unavoidable consequence of the characteristic size of pangolin scales.

3.2. Fractography of dry samples

Images of the sample surface before and after testing for the two orientations are shown Fig. 5. All images are taken from the dorsal side. Transverse samples with cracks propagating parallel to the ridges exhibited brittle-like surface morphologies (Fig. 5a), while some inelastic deformation occurred around cracks in longitudinal samples as evident from the inelastic region surrounding the crack (Fig. 5b). The difference in these two morphologies can be attributed to the available crack paths within the scale due to the orientation of the lamellae. SEM images of the fracture surface (Fig. 6a) reveal internal features consistent with observations made by Liu et al. (2016a) and Wang et al. (2016b). A post-mortem SEM image of an ambient transverse sample reveals the gradual rotation of keratinous lamellae through the thickness of the sample (outlined by dotted lines), consistent with the schematic shown in Fig. 1d. Detailed images of the fracture surface reveal fibrous fracture features in the dorsal region (Fig. 6b), while lamellae in the ventral region exhibit tablet pullout (Fig. 6c). These features are further explored in Section 3.4, where microtomography images of the crack show preferential crack planes for the hydrated samples.

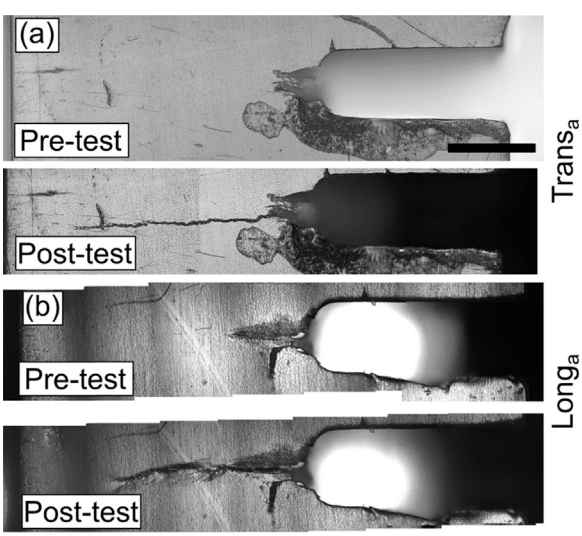

Fig. 5. Composite images of the dorsal surface before and after testing for (a) Trans$_a$ and (b) Long$_a$ samples. Scale bar is 500 μm and is the same for all images. (a) The crack propagates in a brittle-like manner in a Trans$_a$ sample with minimal inelasticity around the crack path. (b) An inelastic region is visible around the crack path in a Long$_a$ sample.

3.3. Influence of hydration on crack toughening

Post-mortem images of hydrated samples reveal more pronounced regions of inelastic damage around the crack path than samples tested in ambient conditions. In particular, a sizeable process zone precedes the crack-tip and leaves behind a wake of inelastic deformation around the crack path (Fig. 7a). Height contours taken from white light interferometry scans on tested samples show depressions at the top of the crack and elevations at the bottom of the crack (Fig. 7b), which coincide with the inelastic region observed in Fig. 7a. The irreversible height change is notable in that it indicates rearrangement of the internal lamellae during crack propagation and an out-of-plane deformation that is consistent with mode mixity arising from the crack deflection inside the sample (as documented in next section), which is a mechanism that contributes to the increased toughness in all samples but that it is more prominent in hydrated samples. Qualitatively, the inelastic process zone is observed to be much larger in the hydrated samples (Fig. 7) relative to the ambient scales (Fig. 5), highlighting the role that water plays in assisting the flow of the keratinous lamellae. Consequently, the hydrated samples are able to sustain a higher fracture resistance, through inelastic toughening.

Within the context of proteinaceous interfaces, increased hydration results in additional hydrogen bonding. As hydrogen bonds are reformable, an increase in their density improves the cohesive behavior of biological interfaces, permitting controlled and extended flow. The effects of hydrogen bonding on interfacial behavior in biological materials are discussed in a recent review from Barthelat et al. (2016) and in keratin-based horse hooves in the work of Bertram and Gosline (1987). With respect to biological role, it is anticipated that this hydration-related toughening behavior increases the *in vivo* survivability of the pangolin scale and acts as a defensive barrier to tooth penetration from the bites of its natural predators.

3.4. Crack deflection – relation to pangolin scale structure

A key observation of the fracture behavior of pangolin scales is the non-uniform crack profile which develops during crack extension. Fig. 8a shows post-mortem optical microscope images from two opposing sides of the same longitudinal sample revealing a pronounced crack extension on the dorsal surface, whereas the ventral surface (Fig. 8b) exhibits a significantly larger inelastic zone with minimal crack extension. In all samples, the crack extension was always longer on the dorsal surface than on the ventral surface, regardless of material orientation or hydration level. That said, the difference in crack length between the two surfaces was higher in longitudinal samples (indicating a less uniform crack front) than in transverse samples. This is likely due to the organization of the lamellae with respect to the crack front, which is more heterogeneous in longitudinal samples than in transverse samples. This mechanism is illustrated by Fig. 8c, where a

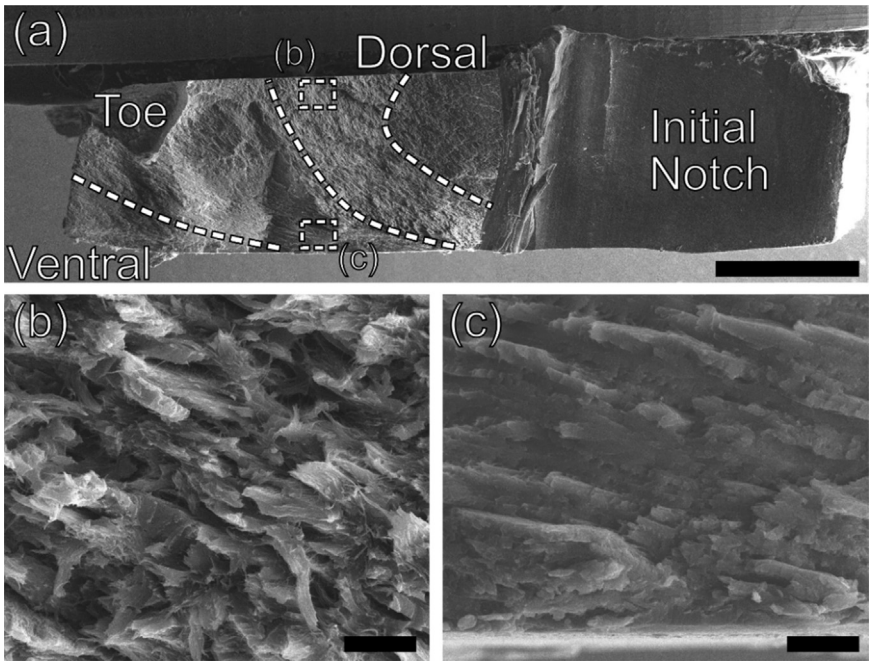

Fig. 6. SEM images of the fracture surface of a transverse sample tested in ambient conditions. The sample was loaded until the crack extended through the width of the sample. (a) Low magnification image of the fracture surface with the orientation of lamellae outlined. The crack propagated from the right to the left in the image. Scale bar is 500 μm. (b) Magnified image of the dorsal layer showing fiber-like pullout of keratinous lamellae. Scale bar is 10 μm. (c) Magnified image of ventral layer showing tablet sliding and fracture. The orientation of the lamellae is nearly parallel with the lower sample surface. Scale bar is 10 μm.

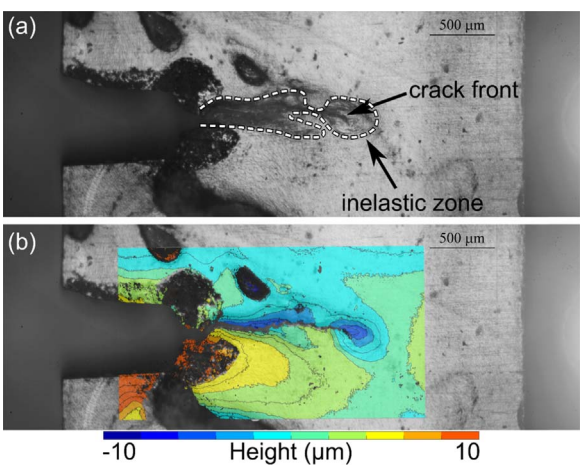

Fig. 7. (a) Composite image of the dorsal side of a $Long_h$ sample showing a larger inelastic zone as compared to ambient conditions. (b) The same image is overlaid with the topology of the sample surface showing depressed regions on the top of the crack and elevated regions below the crack. Isosurface contours are displayed in 1 μm increments and the color scale changes every 2 μm. (For interpretation of the color scheme used in the surface contour plot, the reader is referred to the web version of this article).

crack propagating in a longitudinal sample (shown in blue) is deflected from the vertical plane and preferentially propagates through the interlamellar region. The propagation of the crack in the interlamellar region is thus directed by the dihedral angle, θ, of the angled lamellae. This manner of crack deflection is not accessible to a crack propagating in a transverse sample (shown in red), due to the orthogonal stacking of lamellae with respect to the plane of the crack-tip. The observed interlamellae shearing of the proteinaceous interface (Fig. 6c) results in tablet sliding and inelastic regions surrounding the crack, in a manner similar to that observed in other biomaterials, with the most classical example being nacre (Barthelat and Espinosa, 2007; Espinosa et al., 2011; Espinosa et al., 2009). It should be noted that similar crack deflection mechanisms are expected in the Chinese pangolin, as it is known to possess a similar arrangement of keratinous lamellae within its scales (Wang et al., 2016b). Fig. 8d-f shows different orthographic views of a 3D model of the crack profile taken from microCT images of the sample shown in Fig. 8a, b. The blue voxels represents the free surface of the crack, which exhibits a slanted and discontinuous crack front and the gray voxels contain the pre-notched region. The deflection of the crack in the inter region is best illustrated in Fig. 8f which images the fracture relief along an axis parallel to the propagation direction. These scans support the idea that the crack prefers to propagate between layers of the keratinous lamellae in longitudinal samples and contributes to their increased toughness compared to transverse samples. Additional microCT reconstructions for the $Trans_h$ condition along with animations of both the $Long_h$ and $Trans_h$ crack profile morphologies are provided as Supplementary Material.

4. Conclusions

Pangolin scales are a flexible dermal armor that are comprised of heterogeneous keratinous lamellae structures. Consequently, a crack propagating across a pangolin scale will have a non-uniform profile. Under three-point bend loadings, the crack propagates further within the dorsal region of the material than in the ventral region, though the extent of this non-uniformity depends on both orientation and hydration levels. Standard testing methods were used to calculate lower bound fracture resistance curves of the material while considering this peculiar fracture behavior of the material as a compromise between comparative analysis and representative values. Under inelastic fracture analysis, the toughness of African pangolin scales ranges between ~ 4–6 kJ/m^2 in ambient conditions. The toughness significantly increases by nearly an order of magnitude (~ 25 kJ/m^2) within the measurement window under hydrated conditions. $Long_h$ samples show higher energy dissipation per unit crack length than $Trans_h$ samples, which is attributed to more effective crack deflection in the intermediate layer. These results observed for African pangolins can inform future design principles for improving the toughness of laminated materials.

Acknowledgements

The authors gratefully acknowledge financial support from a Multi-University Research Initiative through the Air Force Office of Scientific Research (AFOSR-FA9550-15-1-0009). We would like to acknowledge Scott Tremor from the San Diego Natural History Museum for providing the pangolin scales. M.D. would like to acknowledge financial support

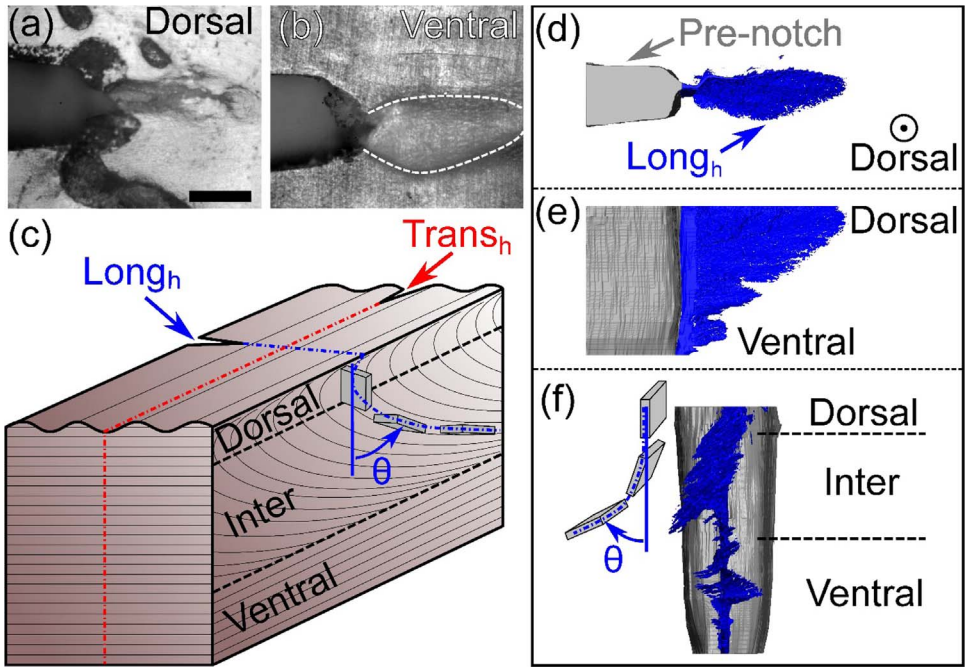

Fig. 8. Influence of lamellae structure on the crack profile of a Long$_h$ sample. (a) Post-mortem image of the crack on the dorsal surface. (b) Post-mortem image of the crack on the ventral surface. The length of the inelastic zone (dashed lines) on the ventral surface is comparable to the length of the crack on the dorsal surface. The scale bar in (a) is 200 μm and (b) is shown at the same magnification. (c) Schematic of the lamellae orientations with preferred crack paths outlined for Long$_h$ (blue) and Trans$_h$ (red, see Supplementary Material) fracture samples. The relative dihedral angles, θ, of the keratinous lamellae are indicated. (d)-(f): 3D reconstruction of microCT images of the crack profile from three orthogonal projections showing fracture surfaces consistent with the orientation of the lamellae structures. Blue and gray voxels represent the crack and pre-notched features, respectively. (For interpretation of the references to color in this figure, the reader is referred to the web version of this article).

under the Postdoctoral Fellowships Program (Application No.: PDF-502224-2017) from the Natural Sciences and Engineering Research Council (NSERC) of Canada. This work made use of the EPIC, Keck-II, and/or SPID facilities of Northwestern University's NUANCE Center.

Appendix A. Supporting information

Supplementary data associated with this article can be found in the online version at http://dx.doi.org/10.1016/j.jmbbm.2017.06.009.

References

Abdel-Aal, H.A., El Mansori, M., 2011. Reptilian skin as a biomimetic analogue for the design of deterministic tribosurfaces. Biol. Med Phys. Biomed. 51–79.
Achrai, B., Wagner, H.D., 2013. Micro-structure and mechanical properties of the turtle carapace as a biological composite shield. Acta Biomater. 9, 5890–5902.
Arciszewski, T., Cornell, J., 2006. Bio-inspiration: learning creative design principia. Lect. Notes Artif. Int. 4200, 32–53.
ASTM(E1820-15a), 2015. Standard Test Method for Measurement of Fracture Toughness. ASTM International, West Conshohocken, PA.
Balani, K., Patel, R.R., Keshri, A.K., Lahiri, D., Agarwal, A., 2011. Multi-scale hierarchy of Chelydra serpentina: microstructure and mechanical properties of turtle shell. J. Mech. Behav. Biomed. 4, 1440–1451.
Barthelat, F., Espinosa, H.D., 2007. An experimental investigation of deformation and fracture of nacre-mother of pearl. Exp. Mech. 47, 311–324.
Barthelat, F., Tang, H., Zavattieri, P.D., Li, C.M., Espinosa, H.D., 2007. On the mechanics of mother-of-pearl: a key feature in the material hierarchical structure. J. Mech. Phys. Solids 55, 306–337.
Barthelat, F., Yin, Z., Buehler, M.J., 2016. Structure and mechanics of interfaces in biological materials. Nat. Rev. Mater. 1.
Bentov, S., Zaslansky, P., Al-Sawalmih, A., Masic, A., Fratzl, P., Sagi, A., Berman, A., Aichmayer, B., 2012. Enamel-like apatite crown covering amorphous mineral in a crayfish mandible. Nat. Commun. 3, 839.
Bertram, J.E.A., Gosline, J.M., 1987. Functional design of horse hoof keratin – the modulation of mechanical-properties through hydration effects. J. Exp. Biol. 130, 121–136.
Boyde, A., 1964. The Structure and Development of Mammalian Enamel. University of London, Queen Mary.
Browning, A., Ortiz, C., Boyce, M.C., 2013. Mechanics of composite elasmoid fish scale assemblies and their bioinspired analogues. J. Mech. Behav. Biomed. 19, 75–86.
Bruet, B.J.F., Song, J.H., Boyce, M.C., Ortiz, C., 2008. Materials design principles of ancient fish armour. Nat. Mater. 7, 748–756.
Chen, I.H., Kiang, J.H., Correa, V., Lopez, M.I., Chen, P.Y., McKittrick, J., Meyers, M.A., 2011. Armadillo armor: mechanical testing and micro-structural evaluation. J. Mech. Behav. Biomed. 4, 713–722.
Chintapalli, R.K., Mirkhalaf, M., Dastjerdi, A.K., Barthelat, F., 2014. Fabrication, testing and modeling of a new flexible armor inspired from natural fish scales and osteoderms. Bioinspir Biomim. 9, 036005.
Damiens, R., Rhee, H., Hwang, Y., Park, S.J., Hammi, Y., Lim, H., Horstemeyer, M.F., 2012. Compressive behavior of a turtle's shell: experiment, modeling, and simulation. J. Mech. Behav. Biomed. 6, 106–112.
Dastjerdi, A.K., Barthelat, F., 2015. Teleost fish scales amongst the toughest collagenous materials. J. Mech. Behav. Biomed. 52, 95–107.
Espinosa, H.D., Juster, A.L., Latourte, F.J., Loh, O.Y., Gregoire, D., Zavattieri, P.D., 2011. Tablet-level origin of toughening in abalone shells and translation to synthetic composite materials. Nat. Commun. 2, 173.
Espinosa, H.D., Rim, J.E., Barthelat, F., Buehler, M.J., 2009. Merger of structure and material in nacre and bone - Perspectives on de novo biomimetic materials. Prog. Mater. Sci. 54, 1059–1100.
Gursoy, D., De Carlo, F., Xiao, X.H., Jacobsen, C., 2014. TomoPy: a framework for the analysis of synchrotron tomographic data. J. Synchrotron Radiat. 21, 1188–1193.
Huang, J.H., Durden, H., Chowdhury, M., 2011. Bio-inspired armor protective material systems for ballistic shock mitigation. Mater. Des. 32, 3702–3710.
Kasapi, M.A., Gosline, J.M., 1997. Design complexity and fracture control in the equine hoof wall. J. Exp. Biol. 200, 1639–1659.
Koizumi, M., Niino, M., 1995. Overview of Fgm research in Japan. Mrs Bull. 20, 19–21.
Krauss, S., Monsonego-Ornan, E., Zelzer, E., Fratzl, P., Shahar, R., 2009. Mechanical function of a complex three-dimensional suture joining the bony elements in the shell of the red-eared slider turtle. Adv. Mater. 21, 407–412.
Liu, Z.Q., Jiao, D., Weng, Z.Y., Zhang, Z.F., 2016a. Structure and mechanical behaviors of protective armored pangolin scales and effects of hydration and orientation. J. Mech. Behav. Biomed. 56, 165–174.
Liu, Z.Q., Jiao, D., Weng, Z.Y., Zhang, Z.F., 2016b. Water-assisted self-healing and property recovery in a natural dermal armor of pangolin scales. J. Mech. Behav. Biomed. 56, 14–22.
Liu, Z.Q., Zhu, Y.K., Jiao, D., Weng, Z.Y., Zhang, Z.F., Ritchie, R.O., 2016c. Enhanced protective role in materials with gradient structural orientations: lessons from Nature. Acta Biomater. 44, 31–40.
Mayer, G., 2005. Rigid biological systems as models for synthetic composites. Science 310, 1144–1147.
Meyers, M.A., Chen, P.-Y., 2014. Biological Materials Science: Biological Materials, Bioinspired Materials, and Biomaterials. Cambridge University Press.
Meyers, M.A., Chen, P.Y., Lin, A.Y.M., Seki, Y., 2008. Biological materials: structure and mechanical properties. Prog. Mater. Sci. 53, 1–206.
Meyers, M.A., Lin, Y.S., Olevsky, E.A., Chen, P.Y., 2012. Battle in the Amazon: Arapaima versus Piranha. Adv. Eng. Mater. 14, B279–B288.
Porter, M.M., Ravikumar, N., Barthelat, F., Martini, R., 2016. 3D-printing and mechanics of bio-inspired articulated and multi-material structures. J. Mech. Behav. Biomed.
Schindelin, J., Arganda-Carreras, I., Frise, E., Kaynig, V., Longair, M., Pietzsch, T., Preibisch, S., Rueden, C., Saalfeld, S., Schmid, B., Tinevez, J.Y., White, D.J., Hartenstein, V., Eliceiri, K., Tomancak, P., Cardona, A., 2012. Fiji: an open-source platform for biological-image analysis. Nat. Methods 9, 676–682.
Seki, Y., Kad, B., Benson, D., Meyers, M.A., 2006. The toucan beak: structure and mechanical response. Mat. Sci. Eng. C.-Bio S 26, 1412–1420.
Sherman, V.R., Quan, H., Yang, W., Ritchie, R.O., Meyers, M.A., 2016. A comparative study of piscine defense: the scales of Arapaima gigas, Latimeria chalumnae and Atractosteus spatula. J. Mech. Behav. Biomed.
Spearman, R., 1967. On the nature of the horny scales of the pangolin. Zool. J. Linn. Soc. 46, 267–273.
Suresh, S., 2001. Graded materials for resistance to contact deformation and damage. Science 292, 2447–2451.
Vernerey, F.J., Barthelat, F., 2014. Skin and scales of teleost fish: simple structure but

high performance and multiple functions. J. Mech. Phys. Solids 68, 66–76.
Wang, B., Yang, W., McKittrick, J., Meyers, M.A., 2016a. Keratin: structure, mechanical properties, occurrence in biological organisms, and efforts at bioinspiration. Prog. Mater. Sci. 76, 229–318.
Wang, B., Yang, W., Sherman, V.R., Meyers, M.A., 2016b. Pangolin armor: overlapping, structure, and mechanical properties of the keratinous scales. Acta Biomater. 41, 60–74.
Yang, W., Chao, C., McKittrick, J., 2013a. Axial compression of a hollow cylinder filled with foam: a study of porcupine quills. Acta Biomater. 9, 5297–5304.
Yang, W., Chen, I.H., Gludovatz, B., Zimmermann, E.A., Ritchie, R.O., Meyers, M.A., 2013b. Natural flexible dermal armor. Adv. Mater. 25, 31–48.
Yang, W., Gludovatz, B., Zimmermann, E.A., Bale, H.A., Ritchie, R.O., Meyers, M.A., 2013c. Structure and fracture resistance of alligator gar (Atractosteus spatula) armored fish scales. Acta Biomater. 9, 5876–5889.
Zhu, D.J., Ortega, C.F., Motamedi, R., Szewciw, L., Vernerey, F., Barthelat, F., 2012. Structure and mechanical performance of a "modern" fish scale. Adv. Eng. Mater. 14, B185–B194.
Zhu, D.J., Szewciw, L., Vernerey, F., Barthelat, F., 2013. Puncture resistance of the scaled skin from striped bass: collective mechanisms and inspiration for new flexible armor designs. J. Mech. Behav. Biomed. 24, 30–40.